Local piezo-response for lead-free Ba$_{0.9}$Ca$_{0.1}$Ti$_{0.9}$Zr$_{0.1}$O$_3$ electro-ceramic by switching spectroscopy

Guillermo Herrera-Pérez[a]*, Isaí Castillo-Sandoval[b], Oscar Solís-Canto[c], Gabriela Tapia-Padilla[a],

Armando Reyes-Rojas[d], Luis Edmundo Fuentes-Cobas[d]

[a]*Consejo Nacional de Ciencia y Tecnología (CONACYT), Centro de Investigación en Materiales Avanzados (CIMAV), Miguel de Cervantes, 120, 31136, Chihuahua, Mexico*
[b]*Centro de Investigación en Materiales Avanzados (CIMAV), Miguel de Cervantes, 120, 31136, Chihuahua, Mexico*
[c]*Laboratorio Nacional de Nanotecnología, Centro de Investigación en Materiales Avanzados (CIMAV), Miguel de Cervantes, 120, 31136, Chihuahua, Mexico*
[d]*Departamento de Física de Materiales, Centro de Investigación en Materiales Avanzados (CIMAV), Miguel de Cervantes, 120, 31136, Chihuahua, Mexico*

Received: June 28, 2016; Revised: November 06, 2017; Accepted: November 23, 2017

The purpose of this work is to determine the effective piezoelectric coefficient (d$_{33}$) and the macro ferroelectric hysteresis behavior for the Ba$_{0.9}$Ca$_{0.1}$Ti$_{0.9}$Zr$_{0.1}$O$_3$ (BCZT). The sample was prepared by the modified Pechini method and it was sintered at 1250 ºC for 5 h. The refinements of X-ray diffraction (XRD) patterns obtained by the Rietveld method suggest a slight degree of tetragonality (c/a = 1.0025) in the perovskite structure. High counting statistics was performed in the two-dimensional grazing incidence 2D-GIXRD characterization by using synchrotron radiation. These results and the Raman spectrum analysis support the XRD interpretation. The morphology reveals a non-homogeneous terrace-type shape with a grain size distribution centered at 13 microns. The switching spectroscopy piezo-response force microscopy was used to obtained the effective d$_{33}$ = 142 pm/V. The soft ferroelectric hysteresis shows a coercive field H$_c$ = 1.3 kV/cm with a saturation polarization P$_s$ = 15.7 µC/cm^2.

Keywords: *Perovskite, Tetragonal, Piezo-response, Ferroelectric properties.*

1. Introduction

Among lead free electro-ceramics with good dielectric and ferro/piezo electric properties, the 0.5Ba(Zr$_{0.2}$Ti$_{0.8}$)O$_3$ - 0.5(Ba$_{0.7}$Ca$_{0.3}$)TiO$_3$ is the most promising binary system for the substitution of commonly commercial PZT[1-3]. As an example, Liu et al.[4] reported a high piezoelectric coefficient d$_{33}$ ~690 pC/N for this binary composition. Scientists have made several efforts to reproduce this value by synthesizing through different routes and controlling density and grain growth[5]. For the Ba$_{0.9}$Ca$_{0.1}$Ti$_{0.9}$Zr$_{0.1}$O$_3$ composition (denoted in this work as BCZT), earlier reports suggest a single perovskite crystal structure with tetragonal phase (P4mm space group, No. 99)[6,7]. In fact, similar compositions that fall in the tricritical point (also called the morphotropic phase boundary) show a strong influence of the tetragonal phase[8,9]. The literature[10,11] suggested that electro-ceramics with similar compositions could exhibit high electrical response when were achieved other physical and microstructural parameters, such as high density (above 96%) and grain size above 15 microns.

The switching spectroscopy piezo-response force microscopy using dual AC resonance tracking (SS-PFM-DART) method has proved to be an important technique to

determine the effective piezoelectric coefficient d$_{33}$ in bulk samples or thin films[11-16]. In the piezo-response mode, a high frequency AC voltage superimposed at on a time variant DC bias voltage is applied to the conductive tip, causes the oscillation of electric dipoles in ferroelectric domains. They oscillate with the same frequency as the applied voltage[17]. The PFM tip as first-harmonic´s resonant contact signal through the tip-sample interaction can detect the amplitude and phase of this oscillation. By plotting the amplitude/phase versus the DC bias voltage, an amplitude butterfly curve and a phase hysteresis loop will be obtained, if the sample is ferroelectric and the applied DC bias voltage is large enough to induce local polarization switching. Generally, the curves are measured at the "OFF" state to characterize the switching behavior, which can minimize the effects of electrostatic interactions[18].

The physical nature of spontaneous polarization in polycrystalline electro-ceramics is an open question that could be approached from the structural and microstructural point of view[19]. Two-dimensional grazing-incidence X-ray diffraction (2D-GIXRD) with an area detector[20] is an important structural characterization technique to determine better diffraction peaks separation and the detection of low level of impurities[21]. It is possible to observe the intensity variations displayed

*e-mail: guillermo.herrera@cimav.edu.mx

along the concentric Debye rings, which are collected with a two-dimensional position sensitive detector [22]. The use of synchrotron radiation as a source for the grazing-incidence X-ray; one can get a very fine- focused high intensity beam with beam size < 5 mm; and one can select a particular wavelength (monochromatic X-ray photons)[21]. The use of an area detector facilitates more rapid collection of intensity across a large section of reciprocal space, resulting in a great decrease in the total acquisition time.

The purpose of this work is to determine the local piezoelectric response d_{33} and the macroscopic ferroelectric parameters for the lead free electro-ceramic $Ba_{0.9}Ca_{0.1}Ti_{0.9}Zr_{0.1}O_3$ (BCZT). Then, these results were associated with the crystal structure and microstructure. Conventional X-ray diffraction pattern was obtained to analyze the lattice parameters by the use of Rietveld method in the Fullprof software. 2D-GIXRD experiments based on synchrotron radiation are presented by the better counting statistics (more intense peaks) leading to better signal-to-noise and signal-to-background ratio and the collection of fluorescence-free data compared to a conventional experiment, in order to detect minority phases. The local d_{33} measurements were derived by SS-PFM in DART mode at room temperature on "OFF" state to minimize the electrostatic contribution. The macroscopic ferroelectric parameters were presented for supporting the electrical properties of this lead-free material. Raman spectroscopy and scanning electron microscopy complement the structural and microstructural characterization of this compound.

2. Experimental Procedure

The BCZT sample was prepared by modified Pechini method. Details of the experimental procedure were previously published[7,23]. Powders of BCZT were heat treated at 700 ºC for 1 h in order to stabilize one phase. Powders were milled for 3 h and they were pressed into pellets of 13.0 mm diameter and 1 mm of thickness. Pellets were sintered at 1250 ºC for 5 h. XRD structure analysis for the bulk was performed by means of a PANalytical XPert´PRO diffractometer equipped with an X´Celerator detector. $\lambda\,(CuK_\alpha) = 1.5406$ Å radiation was used. Diffraction patterns were collected in the 20 - 60º range using step-scanning mode with a step of 0.016º (2θ) and 60 s of step counting time. Lattice parameters and other structural parameters of the BCZT phase were determined by refinement with the profile-matching variant of the Rietveld method using the FULLPROF program version 2017[24]. The refinement involved the following parameters: scale factor, zero displacement correction, unit cell and background parameters, peak profile parameters using a pseudo-Voigt function including the peak asymmetry. Synchrotron 2D-GIXRD with an area detector of beamline 11-3 at Stanford Synchrotron Radiation Laboratory (SSRL) using λ = 0.0976 nm. The incidences angles were 0.1 to 3º. The distance between the sample and the detector was 150

mm. Each diffraction image was acquired varying the time from 1 s to 30 s per spot. The data was calibrated using spectra gotten from LaB_6 and they were analyzed using WxWindows Diffraction Integration Tool version 1.15[25]. Afterwards, they were converted to q_{xy}-q_z, this parameter was later converted to q_{chi}. Finally, q_{chi} was integrated over Chi, and it gave a result of 1-D plot of intensity as a function of the scattering vector q.

The piezoelectric hysteresis loops were also investigated by the SS-PFM method, which was operated in vertical mode with AC driving voltage amplitude of $5V_{pk-pk}$. The drive frequency was 295 kHz in the contact resonance (far of the cantilever´s free resonance), and it was applied between the bottom electrode and the conductive tip during imaging. The AFM tips (Asylum Research, ASYELEC-01 model) are made of Silicon and conductive coating Ti/Ir with thickness of 5/20 nm, respectively. The force constant and the free resonance frequency of the cantilever are 0.2 N/m and 70 KHz, respectively. Local polarization (hysteresis loops) were determined by applying a DC bias voltage from -15 to +15 V_{pk-pk} in DART method at room temperature. For the PFM hysteresis measurements, the first harmonic of the contact resonant frequency was measured. Next, the sum of the pulsed triangular DC bias and the AC driving voltage was performed. This signal was applied to the sample by the tip using an AFM system (MFP-3D, Asylum Research, Oxford Instruments). This pulsed triangular DC bias voltage is used due two kind of hysteresis loops are obtained. The first one is in the DC "ON" state and the other one is in the DC "OFF" state. It is well knowing that the PFM hysteresis loops obtained in the DC "OFF" state contain less electrostatic artifacts than those measured by the DC "ON" state [15,16,26]. For this reason, this work shows the DC "OFF" hysteresis loops. The macroscopic ferroelectric measurements were obtained on the sample previously polished using 800 and 1000 grits SiC paper. The samples were heat treated at 500 ºC for 5 h to remove residual stress due to the polishing process. Colloidal silver paste was painted on the polished surfaces. The samples were heated at 600 ºC for 30 min. The sintered ceramics were poled under 3 kV/mm DC field for 30 min in a silicone oil bath at room temperature. The bulk d_{33} of the ceramics was measured using a piezo-d_{33} meter (Piezo d_{33} Tester Pennebaker 8000 model American Piezo Ceramics Inc.). The ferroelectric properties were measured using a Radian Technologies Precision Workstation, (model P-WS) and high voltage power amplifier TREK (model 609 A, Albuquerque New Mexico, USA).

3. Results and Discussion

Fig. 1 (a) shows the perovskite structure for the electro-ceramic BCZT obtained with Vesta software[27]. The structure depicts the tetragonal distortion due to displacement of Titanium from the center, in order to interact with Oxygen

in the 002 plane. This result is based on the crystallographic information derived through the refinements analysis (using the Rietveld method) performed on the X-ray diffraction pattern (XRD) of BCZT that is presented in panel (b). This panel displays the experimental XRD pattern in dotted line (Y$_{obs}$), collected for a pellet of BCZT sintered at 1250 ºC for 5 h. The panel (b) also displays the Miller indices (hkl). The pattern shows narrow broadened reflections attributed to a single perovskite structure. The broadening reflections suggest a crystal growth in the micro scale. The scanning electron micrographs confirmed this result, as it can be seen in panel (c). The set of reflections, with 2θ (º) values around 22.2, 31.5, 38.8, 45.2, 50.8, 56.1, suggests the presence of a single tetragonal phase (P4mm space group, No. 99). However, the splitting associated to the tetragonal (200)$_t$ crystallographic direction located at around 45.2º is not evident. In order to elucidate the structure associated to this composition, Rietveld refinement analysis was performed by using Fullprof software. Panel (b) also displays the calculated pattern denoted by a solid line (Y$_{calc}$). A good agreement can be observed between the experimental and calculated patterns; considering a single tetragonal phase with P4mm space group. The lattice parameters, Rietveld parameters and the atomic positions are presented in Table I. This information suggests a little distortion of the Titanium cation position with respect to the position of the Oxygen cation [28], with a degree of tetragonality c/a = 1.0025. This value is in agreement with the tetragonal distortion reported by V. S. Puli et al[29]. Consequently, it is necessary to take another approach to confirm the phase identification. The Raman spectroscopy is a supplementary characterization to support this interpretation. Panel (c) shows a representative scanning electron micrograph to evaluate the grain size and shape distribution. Five micrographs were processed with the image J software [30] to generate a histogram. The grain size distribution was centered at 13.1 ± 0.7 μm. Panels (c and d) show a terrace-type morphology with a diversity of grain shapes. This morphology was observed and it was reported previously for BaTiO$_3$. These authors suggest that the formation and presence of terraces is due to the abnormal grain growth during the sintering process[31,32].
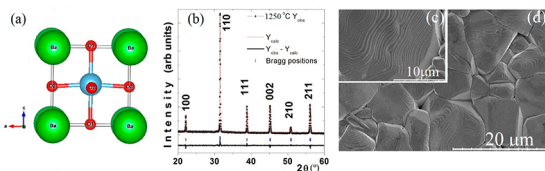

Figure 1. (a) Perovskite type BCZT structure with tetragonal phase. (b) Conventional XRD pattern for BCZT bulk sample sintered at 1250 ºC for 5 h and the comparison with refinement analysis by Rietveld method using Fullprof. (c-d) SEM micrographs reveal a terrace-type morphology in the micro range for the pellet sintered at 1250 ºC for 5 h.

Panel (a) in Fig. 2 shows a representative 2D-GIXRD with an area detector pattern for a pellet with a thickness of 100 nm. This pattern displayed with WxDiff software[25] shown uniform distribution of intensities along the Debye rings. This result clearly suggests a lack of a crystallographic texture. A similar uniform distribution of intensities was observed in other patterns collected with other incidence angles. In panel (a), the Miller indices (hkl) were used to identify different Debye rings. Panels (b and c) show the comparison among the reflections observed in the XRD pattern obtained with Cu K$_\alpha$ radiation and the reflections related to the uni-dimensional grazing incidence XRD pattern through the analysis performed in the Chi-integrated diffracted intensity. 2θ was transformed into full scattering vector Q. The larger statistical significance for this result detects the presence of a second phase labeled by an asterisk, as one can observe in panel (d). This result is associated with the Ba$_{11}$Ti$_{28}$O$_{66.5}$ compound according to the standard PDF card No. 01-073-5502. A. Reyes-Montero et al[6] suggests that the lower sintering temperature in this electro-ceramic could present a small amount of secondary phase that is undetectable by conventional XRD experiments. On the other hand, a broadening of 200 plane was observed respect to the sharper 111 plane suggesting the presence of a structural doublet, which could be associated to the tetragonal phase supporting our XRD and Raman interpretation.
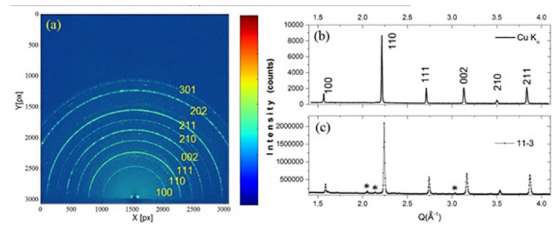

Figure 2. (a) 2D GIXRD pattern for BCZT using an incidence angle of 1º. (b and c) Comparison between the XRD pattern obtained with Cu K$_\alpha$ radiation and the uni-dimensional grazing-incidence X-ray diffraction pattern derived from the panel (a).

The next step of this work was to evaluate the BCZT bulk by Raman spectroscopy at room temperature to confirm the presence of a tetragonal phase as we discussed in the XRD section. The bands in the Raman spectrum displayed in Fig. 3 were labeled according to the irreducible representations (Raman active modes) for P4mm (99) with C$_{4v}^1$ point group. The range of 100-300 cm^{-1} are associated with two A$_1$ transverse optical modes [A$_1$ (TO)] and a longitudinal optical mode [A$_1$ (LO)]. The band around 305 cm^{-1} is characteristic of the tetragonal phase and it is assigned to a combined mode [B$_1$, E (TO + LO)]. This Raman shift corresponds to the asymmetrical vibration mode of TiO$_6$ octahedral. Ba-O bonds produce two mixed modes, [A$_1$, E(TO)] and [A$_1$, E

[LO)], at the high frequencies of about 520 and 725 cm[-1][33]. These results suggest the presence of tetragonal distortion in the BCZT ceramic that are in good agreement with the Rietveld refinement of XRD pattern.
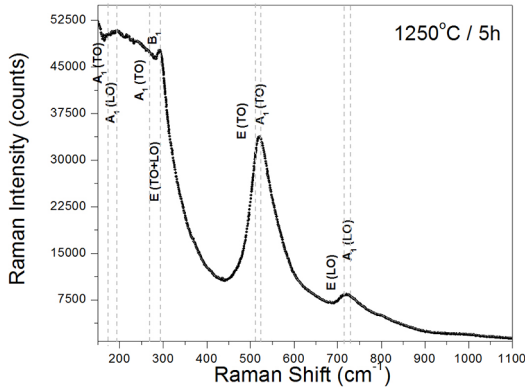

Figure 3. Raman spectra for the sintered BCZT compound. The existence of a peak at 305 cm^{-1} [B[1], E (TO+LO] is a fingerprint for a perovskite structure with tetragonal phase.

The ferroelectricity in BCZT and the switching of the polarization were determined by the use of the switching spectroscopy piezo-response force microscopy technique in DART mode. Figs. 4 (a, b and c) show the topography, PFM amplitude and PFM phase images, respectively. Fig. 4 (d) shows the amplitude versus DC bias voltage, which exhibits the typical butterfly curve, which has information about piezoelectric deformation under an applied DC bias voltage[34]. A PFM Phase versus DC bias voltage plot demonstrates the local polarization switching behavior[35] with a clear hysteresis, as one can observe in Fig. 4 (e). From the butterfly curve showed in panel 4 (d), the effective piezoelectric coefficient (d_{33}) value[35] was estimated through the following equation of the law of converse of piezoelectric effect[32,36-38]:

$$(V - V_1)d_{33} = D - D_1 \qquad (1)$$

where D is the measured value of piezoelectric displacement, V is the applied voltage, and D_1 and V_1 are the piezoelectric displacement and applied voltage of the intersection[32]. Fig. 4 (f) depicts the piezo-response curve as a function of DC bias voltage for BCZT heat-treated at 1250 ºC on one local zone.

The effective piezoelectric coefficient d_{33} obtained for sample BCZT annealing at 1250 ºC is 142.3 pm V[-1] at the maximum voltage of 15 V. The coercive voltage is 3.36 V was evaluated using the equation $(V_c^+ - V_c^-)/2$ where V_c^+ and V_c^- are forward and reverse coercive bias voltages[39].

In order to determine the macroscopic ferro-electrical response for the BCZT bulk material, Fig. 5 shows a clearly hysteresis loop in the P-E plot in where the remnant polarization (P_r) and coercive field (H_c) were determined. One can observe in this panel how increases these values
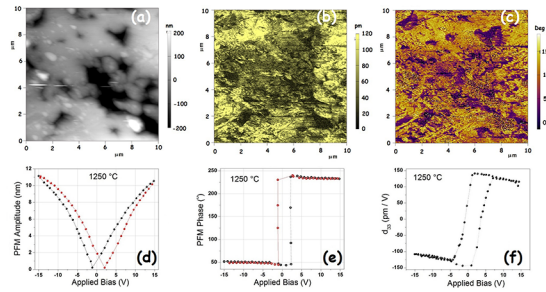

Figure 4. Local ferroelectric domain switching. (a) Topography. (b) PFM amplitude. (c) PFM phase. (d) Local hysteresis loop behavior for the amplitude. (e) Hysteresis loop for the phase component. (f) d_{33} evolution versus DC applied bias voltage.

with increasing applied field from 6 to 9 kV/cm collected at 600 V and 900V. The enclosed area of the hysteresis suggests a soft ferroelectric material, this means an easy polarization of the sample i. e., the sample has H_c of 1.3 kV/cm. The other ferroelectric parameters were the $2P_r = 12$ μC/cm^{2} and the saturation polarization ($P_s = 15.7$ μC/cm^{2}). The change in coercive field obtained in electrical polarization-voltage (P-V) measurement compared with the PFM P-V characterization is probably due to the difference in the electrical boundary conditions at the local top electrodes[40] (measurements were taken using a Ti/Ir coated tip for the PFM and Al for the electrical P-E). The poled ceramic shows a bulk d_{33} around 232 pC/N. This value is comparable with the bulk d_{33} obtained by A. Reyes et al[6] and K. Castkova et al[41]. The local piezo-response and the macroscopic ferroelectric behavior observed in this sample is in agreement with the global tetragonal structure formed, as it can be observed in the XRD 2D-GIXRD and Raman sections.
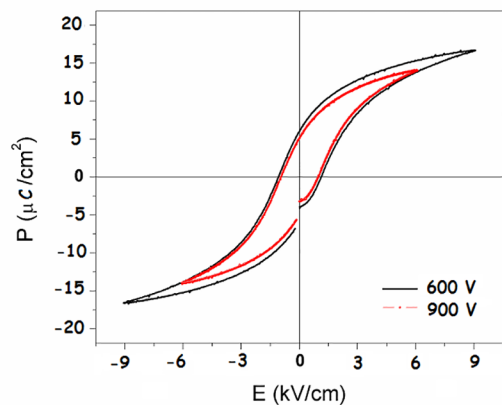

Figure 5. Macroscopic polarization -voltage hysteresis for the BCZT heat-treated at 1250 ºC for 5h.

4. Conclusions

In summary, this work shows evidence of the local piezo-electric response (effective d_{33}) and macroscopic ferroelectricity in the lead-free perovskite polycrystalline $Ba_{0.9}Ca_{0.1}Ti_{0.9}Zr_{0.1}O_3$

prepared by modify Pechini method. These characterizations were performed on a sintered sample (1250 ºC for 5h) that reveals a grain size distribution centered at 13 microns. The effective d$_{33}$ = 142 pm/V was determined by switching spectroscopy piezo-response force microscopy in DART mode on "OFF" state. The bulk d$_{33}$ = 232 pC/N and the soft ferroelectric hysteresis parameters such as H$_c$ = 1.3 kV/cm and P$_s$ = 15.7 µC/cm^2 were associated with the tetragonal distortion (P4mm space group; No. 99; C$_{4V}^1$) in perovskite structure. The lattice parameters and the atomic positions were analyzed by the Rietveld refinement of XRD patterns using Fullprof software. The degree of tetragonality value was 1.0025. The high counting statistics (in the 2D-GIXRD patterns using synchrotron radiation) in combination with the Raman results support the interpretation performed in the conventional XRD patterns. More research about the preparation of the samples and the influence of the structure and microstructure on the piezo/ferroelectric properties of BCZT is being carried out.

5. Acknowledgments

6. References

1. Shrout TR, Zhang SJ. Lead-free piezoelectric ceramics: Alternatives for PZT? *Journal of Electroceramics*. 2007;19:113-126.

2. Coondoo I, Panwar N, Amorín H, Alguero M, Kholkin AL. Synthesis and characterization of lead-free 0.5Ba(Zr$_{0.2}$Ti$_{0.8}$)O$_3$-0.5(Ba$_{0.7}$Ca$_{0.3}$)TiO$_3$ ceramic. *Journal of Applied Physics*. 2013;113(21):214107.

3. Coondoo I, Panwar N, Kholkin A. Lead-free piezoelectrics: Current status and perspectives. *Journal of Advanced Dielectrics*. 2013;3:1330002.

4. Liu W, Ren X. Large Piezoelectric Effect in Pb-Free Ceramics. *Physical Review Letters*. 2009;103(25):257602.

5. Villafuerte-Castrejón ME, Morán E, Reyes-Montero A, Vivar-Ocampo R, Peña-Jiménez JA, Rea-López SO, et al. Towards Lead-Free Piezoceramics: Facing a Synthesis Challenge. *Materials*. 2016;9(1):21-48.

6. Reyes-Montero A, Pardo L, López-Juárez R, González AM, Cruz MP, Villafuerte-Castrejón ME. Lead-free Ba$_{0.9}$Ca$_{0.1}$Ti$_{0.9}$Zr$_{0.1}$O$_3$ piezoelectric ceramics processed below 1300 ºC. *Journal of Alloys and Compounds*. 2014;584:28-33.

7. Herrera-Pérez G, Morales D, Paraguay-Delgado F, Borja-Urby R, Reyes-Rojas A, Fuentes-Cobas LE. Structural analysis, optical and dielectric function of [Ba$_{0.9}$Ca$_{0.1}$](Ti$_{0.9}$Zr$_{0.1}$)O$_3$ nanocrystals. *Journal of Applied Physics*. 2016;120(9):094303.

8. Ye S, Fuh J, Lu L, Chang Yl, Yang JR. Structure and properties of hot-pressed lead-free (Ba$_{0.85}$Ca$_{0.15}$)(Zr$_{0.1}$Ti$_{0.9}$)O$_3$ piezoelectric ceramics. *RSC Advances*. 2013;3(43):20693-20698.

9. Venkata Ramana E, Mahajan A, Graça MPF, Mendiratta SK, Monteiro JM, Valente MA. Structure and ferroelectric studies of (Ba$_{0.85}$Ca$_{0.15}$)(Ti$_{0.9}$Zr$_{0.1}$)O$_3$ piezoelectric ceramics. *Materials Research Bulletin*. 2013;48(10):4395-4401.

10. Praveen JP, Karthik T, James AR, Chandrakala E, Asthana S, Das D. Effect of poling process on piezoelectric properties of sol-gel derived BZT-BCT ceramics. *Journal of European Ceramic Society*. 2015;35(6):1785-1798.

11. Li B, Ehmke MC, Blendell JE, Bowman KJ. Optimizing electrical poling for tetragonal, lead-free BZT-BCT piezoceramic alloys. *Journal of European Ceramic Society*. 2013;33(15-16):3037-3044.

12. Li J, Li JF, Yu Q, Chen QN, Xie S. Strain-based scanning probe microscopies for functional materials, biological structures, and electrochemical systems. *Journal of Materiomics*. 2015;1(1):3-21.

13. Bonnell DA, Kalinin SV, Kholkin AL, Gruverman A. Piezoresponse Force Microscopy: A Window into Electromechanical Behavior at the Nanoscale. *MRS Bulletin*. 2009;34(9):648-657.

14. Kholkin AL, Kalinin SV, Roelofs A, Gruverman A. Review of Ferroelectric Domain Imaging by Piezoresponse Force Microscopy. In: Kalinin S, Gruverman A, eds. *Scanning Probe Microscopy - Electrical and Electromechanical Phenomena at the Nanoscale*. Volume II. Chapter 1.6. New York: Springer; 2007. p. 173-214.

15. Jesse S, Baddorf AP, Kalinin SV. Dynamic behaviour in piezoresponse force. *Nanotechnology*. 2006;17(6):1615-1628.

16. Jesse S, Baddorf AP, Kalinin SV. Switching spectroscopy piezoresponse force microscopy of ferroelectric materials. *Applied Physics Letters*. 2006;88(6):062908.

17. Edwards D, Brewer S, Cao Y, Jesse S, Chen LQ, Kalinin SV, et al. Local Probing of Ferroelectric and Ferroelastic Switching through Stress-Mediated Piezoelectric Spectroscopy. *Advanced Materials Interfaces*. 2016;3(7):1500470.

18. Miao H, Sun Y, Zhou X, Li Y, Li F. Piezoelectricity and ferroelectricity of cellular polypropylene electrets films characterized by piezoresponse force microscopy. *Journal of Applied Physics*. 2014;116(6):066820.

19. Baker JL, Jimison LH, Mannsfeld S, Volkman S, Yin S, Subramanian V, et al. Quantification of Thin Film Crystallographic Orientation Using X-ray Diffraction with an Area Detector. *Langmuir*. 2010;26(11):9146-9151.

20. Wenk H, Grigull S. Synchrotron texture analysis with area detectors. *Journal of Applied Crystallography*. 2003;36:1040-1049.

21. Kocks UF, Tomé CN, Wenk HR. *Texture and Anisotropy - Preferred Orientations in Polycrystals and their Effect on Materials Properties*. Cambridge: Cambridge University Press; 1998.

22. Fuentes-Cobas LE. Synchrotron Radiation Diffraction and Scattering in Ferroelectrics. Chapter 6. In: Pardo L, Ricote J, eds. *Multifunctional Polycrystalline Ferroelectric Materials - Processing and Properties*. Dordrecht: Springer; 2011. p. 217-280.

23. Herrera-Pérez G, Morales D, Paraguay-Delgado F, Hurtado-Macias A, Borja Urby R, Tapia-Padilla G, et al. Low loss Electron Energy Spectroscopy Characterization of Electronic Structure and Piezo-response of $Ba_{0.9}Ca_{0.1}Ti_{0.9}Zr_{0.1}O_3$ Nanocrystals. *Microscopy and Microanalysis*. 2016;22(Suppl 3):1908-1909.

24. Rodriguez-Carvajal J. Recent advances in magnetic structure determination by neutron powder diffraction. *Physica B: Condensed Matter*. 1993;192(1-2):55-69.

25. Mannsfeld SC. Stanford Synchrotron Radiation Lightsource, 2009, http://code.google.com/p/wxdif

26. Hong S, Woo J, Shin H, Jeon JU, Pak YE, Colla EL, et al. Principle of ferroelectric domain imaging using atomic force microscope. *Journal of Applied Physics*. 2001;89(2):1377-1386.

27. Momma K, Izumi F. VESTA 3 for three-dimensional visualization of crystal, volumetric and morphology data. *Journal of Applied Crystallography*. 2011;44:1272-1276.

28. Harada J, Pedersen T, Barnea Z. X-ray and neutron diffraction study of tetragonal barium titanate. *Acta Crystallographica Section A: Foundations and Advances*. 1970;A26:336-344.

29. Puli VS, Kumar A, Chrisey DB, Tomozawa M, Scott JF, Katiyar RS. Barium zirconate-titanate/barium calcium-titanate ceramics via sol-gel process: novel high-energy-density capacitors. *Journal of Physics D: Applied Physics*. 2011;44(39):395403.

30. *ImageJ 1.47*. National Institutes of Health, USA. Available from: <http://imagej.nih.gov/ij>. Access in: 30/11/2017.

31. Kästner G, Wagner R, Hilarius V. Nucleation of twins by grain coalescence during the sintering of $BaTiO_3$ ceramics. *Philosophical Magazine A*. 1994;69(6):1051-1071.

32. Lee HY, Kim JS, Hwang NM, Kim DY. Effect of sintering temperature on the secondary abnormal grain growth of $BaTiO_3$. *Journal of the European Ceramic Society*. 2000;20(6):731-737.

33. Venkateswaran UD, Naik VM, Naik R. High-pressure Raman studies of polycrystalline $BaTiO_3$, *Physical Review B*. 1998;58(21):14256.

34. Chen Z, Huang J, Yang Y, Wang Y, Wu Y, He H, et al. Piezoelectric properties of rhombic $LiNbO_3$ nanowires. *RSC Advances*. 2012;2(19):7380-7383.

35. Denning D, Guyonnet J, Rodriguez BJ. Applications of piezoresponse force microscopy in materials research: from inorganic ferroelectrics to biopiezoelectrics and beyond. *International Materials Reviews*. 2016;61(1):46-70.

36. Roelofs A, Schneller T, Szot K, Waser R. Toward the limit of ferroelectric nanosized grains. *Nanotechnology*. 2003;14(2):250.

37. Bharathi P, Thomas P, Varma KBR. Piezoelectric properties of individual nanocrystallites of $Ba_{0.85}Ca_{0.15}Zr_{0.1}Ti_{0.9}O_3$ obtained by oxalate precursor route. *Journal of Materials Chemistry C*. 2015;3(18):4762-4770.

38. Bhimireddi R, Ponraj B, Varma KBR. Structural, Optical, and Piezoelectric Response of Lead-Free $Ba_{0.95}Mg_{0.05}Zr_{0.1}Ti_{0.9}O_3$ Nanocrystalline Powder. *Journal of the American Ceramic Society*. 2016;99(3):896-904.

39. Kang HB, Chang J, Koh K, Lin L, Cho YS. High Quality Mn-Doped $(Na,K)NbO_3$ Nanofibers for Flexible Piezoelectric Nanogenerators. *ACS Applied Materials & Interfaces*. 2014;6(13):10576-10582.

40. Kalinin SV, Rodriguez BJ, Jesse S, Chu YH, Zhao T, Ramesh R, et al. Intrinsic single domain switching in ferroelectric materials on a nearly ideal surface. *Proceedings of the National Academy of Sciences of the United States of America*. 2007;104(51):20204-20209.

41. Castkova K, Maca K, Cihlar J, Hughes H, Matousek A, Tofel P, et al. Chemical Synthesis, Sintering and Piezoelectric Properties of $Ba_{0.85}Ca_{0.15}Zr_{0.1}Ti_{0.9}O_3$ Lead-Free Ceramics. *Journal of the American Ceramic Society*. 2015;98(8):2373-2380.